Check for updates

Design, implementation and piloting of an integrated hydrogen- and oxygen-added process for conversion of biogas to methanol

Carl Fritsch, [iD] *[a] Jule Blankenstein,[a] Benedikt Bender,[b] Jürgen Dornseiffer,[c] Moritz Haep[a] and Kristoffer Ooms[d]

An integrated biogas-to-methanol (B2M) conversion system combining autothermal reforming (ATR) with regenerative methanol (MeOH) synthesis, integrating both oxygen (O_2) and hydrogen (H_2) from water electrolysis, is designed, commissioned and investigated operationally. The pilot plant is operated under real world conditions at a wastewater treatment plant in western Germany to demonstrate the process using sewage-derived biogas and to investigate its applicability and suitability for decentralized, efficient value-added bio-chemical production from renewable feedstock. The studies conducted at the test plant evaluate system effectiveness by optimizing operational parameters for both ATR (steam-to-carbon ratio [S/C], oxygen-to-fuel ratio [λ]) and the methanol (MeOH) synthesis process (stoichiometric number [SN], reaction temperature and gas space velocity [GHSV]). Additionally, stable start-up procedures are developed for reliable operation under dynamic conditions, as is expectable in industrial process application. To compare different MeOH synthesis pathways, regenerative synthesis gas-based MeOH-production is set against direct CO_2-to-MeOH conversion. Results demonstrate that ATR of biogas produces CO_2-rich synthesis gas (SynGas) with excellent methane (CH_4) conversion and extremely low soot formation at relatively low reforming temperatures below 750 °C. Although the high CO_2-content reformate requires substantial H_2 injection for stoichiometric MeOH synthesis SynGas conditions, the H_2-enhanced SynGas route proves superior to CO_2-only operation of the pilot plant, highlighting possible synergies in oxygen-injected ATR and MeOH-synthesis applications. The combined ATR-H_2-injection approach yields higher MeOH yields with reduced water formation and improved conversion. The findings from this study support the technical feasibility of the integrated B2M-system and provide operational foundations for economically viable decentralized MeOH-production at biogas facilities and future system scale-up.

1 Introduction

In order to reduce anthropogenic climate impact, the transition away from fossil resources is imperative. In addition to the widely discussed energy transition, this also includes the transition away from fossil-based material production. Industries that depend heavily on fossil carbon feedstock face significant challenges in their transition toward defossilization. Against this backdrop, biomass has emerged as one of the most promising alternative feedstocks for reducing fossil resource dependency, offering diverse valorization pathways to create viable substitutes within existing carbon-based production systems and value chains.[1] Within this context, bio-waste assumes particular significance. Unlike conventional biomass sources, its availability remains fundamentally decoupled from production infrastructures that compete for limited land resources with sectors such as agriculture and nutrition, which themselves rely substantially on biomass availability.[2] In Germany, historical subsidy frameworks have significantly shaped the utilization of biomass and bio-waste as carbon sources, predominantly favoring fermentation, biogas production, and subsequent combustion for electricity and heat generation.[3] While this approach represents an effective biomass utilization strategy, it inherently sacrifices the renewable carbon potential, thereby precluding downstream material carbon applications unless supplemented by sophisticated carbon-capture technologies. The direct use of biogas in value-added material conversion systems therefore presents an opportunity for the efficient use of available infrastructures towards substitutional

[a]*Forschungsinstitut für Wasserwirtschaft und Klimazukunft an der RWTH Aachen e.V., An der Ölmühle 4, 52074 Aachen, Germany. E-mail: fritsch@fiw.rwth-aachen.de; Tel: +49 241 802 39 55*

[b]*OWI Science for Fuels gGmbH, Kaiserstraße 100, 52134 Herzogenrath, Germany*

[c]*Institute of Energy Materials and Devices IMD-2, Forschungszentrum Jülich GmbH, Wilhelm-Johnen-Straße, 52428 Jülich, Germany*

[d]*Emschergenossenschaft, Kronprinzenstraße 24, 45128 Essen, Germany*

utilization of accessible, regenerative carbon sources in otherwise heavily fossil-reliant industries.[4]

There are many different process routes for material biomass and bio-carbon valorization. One possible application of biomass as a substitute in historically fossil-heavy value chains is the generation of hydrogen-rich synthesis gas (SynGas). In this respect, biomass can be used as a substitute for coal in gasification-processes for generation of carbon-dioxide (CO_2) rich SynGas.[5] Alternatively, certain types of biomass can be converted to biogas through fermentation or fouling processes in order to obtain biogas, a varying mixture of CH_4 and CO_2.[6] Biogas in turn can be used as a substitute in reforming processes, which otherwise utilize CH_4-rich natural gas for production of SynGas.[7] In this context, the production of SynGas-based fuels and chemicals offers a wide range of possibilities for material utilization of biogas and the production of renewable bio-chemicals towards the defossilization of the SynGas- and fuel-industries.[8]

One of the most widely applied, SynGas-derived chemicals is methanol (MeOH).[9] Its wide range of applications as a base chemical, monomer, energy- or hydrogen-carrier and fuel or fuel-substitute makes it one of the most commonly traded petrochemical products in the world today, with about 100 Mt being produced and shipped each year.[10] The possibilities for regenerative MeOH-production thus promise to assume key roles in the global transition away from fossil resources.[11] While regenerative production paths for MeOH have been the focus of many studies in recent years and some preliminary industrial-scale demonstrations have been reported upon, many technical and economical challenges still prevail on our path towards an efficient, global industrial-scale regenerative MeOH-production infrastructure.[12,13] Economically, biogas valorization towards SynGas-production with subsequent conversion to MeOH has the potential to become a cost-effective production route for regenerative MeOH.[14] Thus, the integrated process of reforming biogas to SynGas with possible downstream applications such as MeOH-synthesis has been reported upon often in the recent past, mainly in techno-economic, model-based assessments of possible configurations, and ecological and economical aspects of process design.[11,13,15–23] While principally and technically possible, no integrated large-scale application for this process has been demonstrated commercially to this day. This can be attributed to – among others – three factors:

(1) Biogas can be converted to SynGas through reforming, but – in most cases – the resulting SynGas does not contain enough H_2 for stoichiometric conversion of CO_2 and carbon-monoxide (CO) to MeOH.[11,24,25] This is highly dependent on the Biogas feed composition. For effective and complete carbon conversion, process adaptions have to be made to supply the necessary H_2 to the process and bridge the stoichiometric deficit.

(2) In conventional steam methane reforming (SMR), the high temperatures necessary for effective catalytic generation of SynGas are supplied through partial stream combustion of the input natural gas. As biogas contains high percentages of CO_2, the reduced heating value (HHV) results in higher amounts of input gas being combusted to generate sufficient reforming

heat – some report up to 50% of the total biogas input being used for heating purposes.[26,27]

(3) Biogas – especially in Germany – is produced mainly in decentralized facilities.[28,29] This poses a number of economical challenges of scale for the allocation and efficient conversion of gas streams for industrial production of SynGas and its daughter products such as MeOH.[2,15]

To address these factors, we suggest a combined process approach for O_2-added, autothermal biogas reforming with subsequent H_2-injected conversion of the resulting SynGas to MeOH. This approach combines the commonly reported on, electricity-based E–MeOH production route with a more conventional gas-reforming-based Bio–MeOH approach. We design a system that utilizes biogas or sewage gas for autothermal reforming (ATR) to SynGas.

Here, we use pure O_2 from water electrolysis to supply the reforming unit with an oxidizing agent for catalytic partial oxidation of the CH_4 contained in the input biogas stream. While conventional SMR utilizes a partial gas stream for combustion in an auxiliary firing unit, in our autothermal approach no biogas is used for auxiliary firing and heat production. Instead, the CH_4 is oxidized partially in the catalytic reforming unit, sustaining the necessary internal heat for the reaction between CH_4 and H_2O (1) and supplying all the necessary heat for input H_2O-vaporization and reactant pre-heating. In this way, no regenerative carbon is lost to combustion, but is instead converted entirely to SynGas for subsequent upgrading to MeOH.

As the resulting SynGas does not have stoichiometric proportions of H_2, CO and CO_2, we take advantage of the synergies in electrolysis and use pure H_2 to inject into the SynGas, thus creating more suitable stoichiometric conditions for carbon-oxide conversion to MeOH.

We design and commission a pilot plant for demonstrating the integrated process at the waste water treatment plant (WWTP) 'Emschermündung' in western Germany with a nominal load of 4 $Nm^3\ h^{-1}$ biogas feed and optimize the process operationally, featuring both independent operation of the ATR and the MeOH-synthesis loop as well as combined operation of the two thermochemical systems. We apply novel catalysts both for reforming as well as MeOH-synthesis, proving the potential of the approach. In designing and operating the pilot plant, we investigate the applicability of such a combined, integrated bio-feedstock and electricity based process application under real world operational conditions, probing its suitability as a value added alternative to biogas-combustion for electricity and heat generation. In a first-time process-integration, we explore the adequacy of biogas ATR for producing SynGas for further thermochemical conversion to value added bio-products. Focusing on future demonstration and piloting of MeOH-synthesis, we highlight the operative aspects and limitations of synthesis operation and identify operational and efficiency shortcomings in the process that have to be resolved for future process application and stable, effective operation of related processes. Herein, we identify challenges in start-up and steady-state operation of the system and discuss obstacles towards further scale-up and possible

industrial application of the process in a decentralized environment.

2 State-of-the-art, pilot plant design and set-up

ATR of Biogas as well as MeOH-synthesis from renewable sources have both been demonstrated separately in selected studies in the recent past, highlighting the applicability of both partial systems individually and providing insights into possible system combination for regenerative MeOH-synthesis applications. Nonetheless, no combined approach of autothermal, pure oxygen-injected biogas reforming with hydrogen injected, bio–MeOH synthesis has been reported to date on a pilot scale. The current state of the art was thus used for our design and implementation of the herein reported pilot plant application of the combined process.

ATR of biogas towards H_2- or SynGas-production has been demonstrated prominently by Rau et al., who built a test plant and later carried on to demonstrate the reforming process on a semi-industrial scale.[14,30] Rau et al. used air for partial oxidation of CH_4. This introduces a large amount of nitrogen (N_2) into the system, which is counteractive at the process level for subsequent MeOH-synthesis as a result of the increase in the inert gas mass and the increase in the energy demand for reforming based upon this gas introduction into the thermochemical system. For production of H_2 from the resulting SynGas, where Bio-H_2 has to be separated after reforming, this N_2 will be omitted from the product gas, as was demonstrated in the cited studies. In subsequent SynGas applications such as MeOH-synthesis, this poses an additional obstacle, where inert gas is introduced into a synthesis loop and increases energy demand for pumping, compression and system tempering in steady-state operation.[31] Considering these design limitations, ATR-processes show improved effectiveness and improved efficiency, when operated in oxygen-only environments.[32]

Furthermore, autothermal reforming of synthetic biogas has been investigated in small laboratory scale applications in multiple studies, including Luneau et al., Rathod & Bhale, Guerrero et al. and Hou et al., proving the efficiency potential of the application.[33–36] Luneau et al. showed significant catalyst deactivation at S/C = 3 and λ = 0.5 after just 30 h on-stream, proving that excessive water-injection and subsequent high necessary oxygen-injection rates were able to oxidize the reforming catalyst surfaces and lead to premature deactivation of the applied catalyst formulae.[33] While proving the applicability of the process in principle, in our work we therefore aimed to reduce both water vapor injection and the reduction of λ necessary to achieve suitable reforming temperatures. Meanwhile, Rathod et al. showed that increased temperatures above 650 °C were able to significantly improve CH_4-conversion in their autothermal, dry-reforming laboratory set up with minimization of H_2O-vapor production in the process and maximization of H_2-yield, highlighting noble-metal activity in the activation and conversion of CH_4. For improved process stability, autothermal reforming with H_2O injection was chosen

in this work, applying a noble-metal catalyst and reported temperature ranges with H_2O being able to additionally improve CH_4-conversion and H_2-yield through the SMR-reaction scheme (1).[37] Guerrero et al. showed very high CH_4 and CO_2 conversion in their autothermal partial oxidation reactor, converting most of the injected CH_4, CO_2 and O_2 at temperatures up to 1.500 K through enabling the dry reforming reaction (4).[35] While this approach is able to realize good conversion ratios, the lack of H_2O-vapor and the high reforming temperatures strongly suggest co-production of soot, which acts counter actively in subsequent compression and synthesis processes.[38] Reaction parametrization for ATR with low soot production, good CH_4-conversion and H_2-yield as well as acceptable CO_2-levels in the produced reformate was shown in an extensive equilibrium-study by Nourbakhsh et al., who defined good operational spaces for oxidative SMR under atmospheric pressures.[39]

Hou et al. highlighted the importance of space-velocity in CH_4-reforming under dosing of CO_2 and O_2, leading to a reactor design accommodating GHSV lower than 54.000 h^{-1}.[36]

In addition to this, Topsoe has demonstrated electrified SMR with subsequent conversion to MeOH in a proprietary process (eSMR Methanol).[40] Here, excess grid electricity can be used to supply the necessary heat for the reforming reaction, providing a suitable option for grid balancing. This is an alternative use of electricity integration into the thermochemical B2M-process, but it does not accommodate H_2-deficiency in regenerative MeOH-production based upon high CO_2-content input streams.

Meanwhile, decentralized MeOH-synthesis has been demonstrated in direct CO_2-hydrogenation processes by Carbon Recycling International (CRI), who aim to produce E–MeOH on an economically viable industrial scale in several plants internationally.[20] In the large-scale research project Carbon2Chem, a demonstrator for the decentralized conversion of CO_2 from cement production processes to MeOH was operated in Oberhausen.[41] Both approaches apply CO_2-only input streams, making CO_2-removal feasible in hard to abate sectors, providing a value-added option for effective CO_2-capture and conversion (CCU). In both cases the produced MeOH will not be regenerative in nature, utilizing fossil carbon sources for production of the C1-product.

In a comparable manner to the herein presented work, researchers from DTU Copenhagen piloted a process combining dry and wet reforming of biogas for further conversion to MeOH.[42] Here they applied their 'bio-reforming' unit, able to reform biogas through SMR to regenerative SynGas. Their bio-reforming process was able to convert CO_2 from biogas to CO and H_2, making additional injection of hydrogen optional. The two stage process requires an additional reforming unit for effective conversion of CO_2. If H_2 is additionally injected, no process-synergies for the effective integration of the O_2-product from water-electrolysis are available, reducing the system efficiency for any associated electrolysis. The process was developed concurrently to the herein presented process.

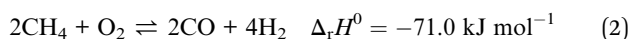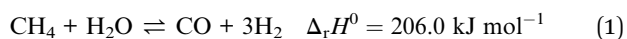Additionally, small-scale MeOH-synthesis from Biogas in three-phase reactors has been reported on by Schipek et al.

recently.[43] Here, a complex three-phase reactor is applied, improving conversion efficiencies, but necessitating the design of an integrated system and complicating the overall system composition.

The herein presented work aims to simplify decentralized MeOH-synthesis, making commercial technologies like reactor setup and catalyst design available to possible future small-scale producers.

Extending upon the existing work, we designed a system for simple, atmospheric conversion of biogas to SynGas in a single-stage ATR-unit applying robust noble-metal catalysts. SynGas is cooled and compressed for subsequent introduction into the MeOH-synthesis loop, utilizing a set of tubular isothermal fixed-bed reactors, product sequestration and gas recycling to yield a regenerative raw MeOH product.

2.1 Design and setup of the autothermal reforming unit

For the production of SynGas from Biogas/Sewage gas, a unit for oxygen-added autothermal reforming was designed and applied. Here, CH_4 and CO_2 from sewage gas as well was H_2O-vapor and O_2 are supplied to a catalytic reactor, where four main catalytic reactions take place simultaneously:

$$CH_4 + H_2O \rightleftharpoons CO + 3H_2 \quad \Delta_r H^0 = 206.0 \text{ kJ mol}^{-1} \quad (1)$$

$$2CH_4 + O_2 \rightleftharpoons 2CO + 4H_2 \quad \Delta_r H^0 = -71.0 \text{ kJ mol}^{-1} \quad (2)$$

$$CO + H_2O \rightleftharpoons CO_2 + H_2 \quad \Delta_r H^0 = -41.2 \text{ kJ mol}^{-1} \quad (3)$$

$$CO_2 + CH_4 \rightleftharpoons CO + 2H_2 \quad \Delta_r H^0 = 247.0 \text{ kJ mol}^{-1} \quad (4)$$

The thermal energy and subsequent reaction temperatures in the system are supplied through partial oxidation of CH_4 to CO and H_2 (eqn (2)). To enable this reaction, pure O_2 is supplied to the catalytic reactor, with temperatures of the resulting reformate being used in a combined heat exchanger (HEX 950) for vaporization of feed water and preheating of the sewage gas. While part of the reaction network in ATR, dry reforming (eqn (4)) can be mostly disregarded in the temperature range tested herein.[14,33] Decomposition of CH_4 to C, Boudouard-decomposition of CO to C and CO_2 reduction were not observed in preliminary laboratory testing of the reformer and are unlikely at the temperature ranges below 700 °C.[44,45] In the overall application of the pilot plant, sewage gas was supplied through an activated carbon filter for the elimination of sulfuric compounds, entering a three-way valve. This allowed for the operation of the system using synthetic gas from gas cylinder bundles instead of raw sewage gas.

The feed gas was pumped into the system using a double membrane pump with cooled pump bodies and pump heads (KNF N2400 ST13.E). Coolant was supplied in the form of mains water from the central pilot plant water supply. (Synthetic) Sewage gas was passed through an additional activated carbon filter for elimination of surplus sulfur and siloxanes, while hydrogen sulfide content was continuously monitored using a gas monitoring unit (ExTox ET-4D, Germany). Mains water was supplied centrally to both the integrated reforming unit as well as the MeOH-synthesis system. Part of the mains water was run through a demineralization unit for elimination of ions in the supplied water. Deionized water was collected and then pumped into the HEX 950. Here it was vaporized, overheated and mixed with the educt sewage gas. The mixed and preheated
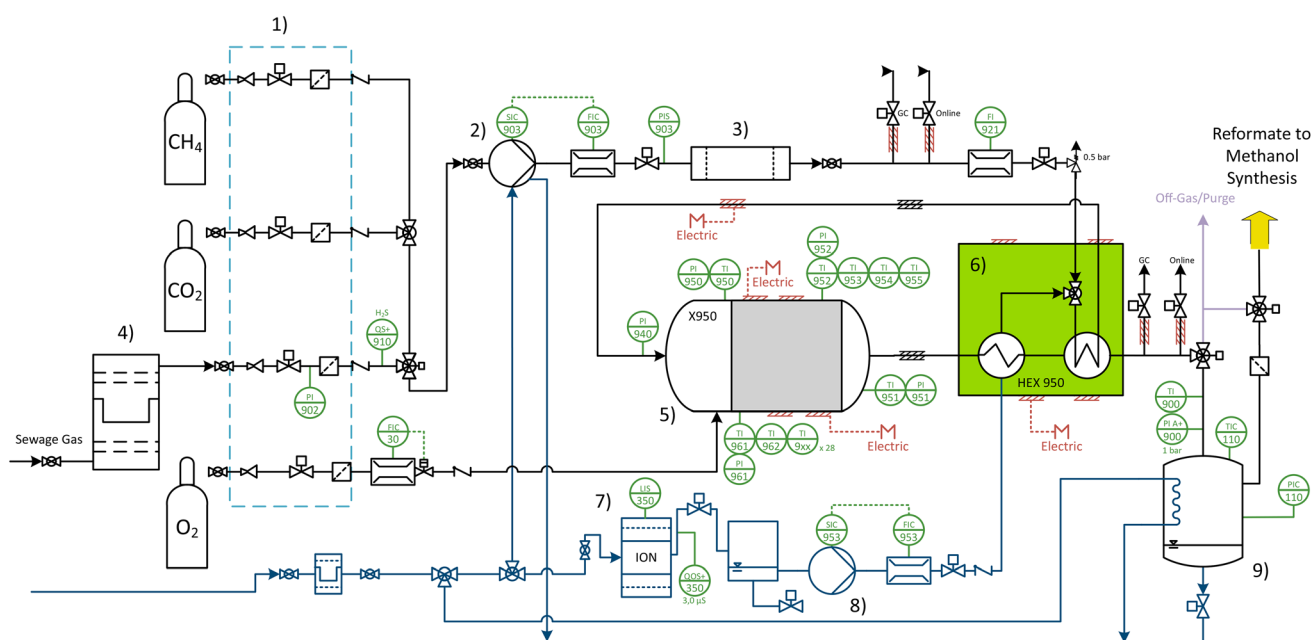

Fig. 1 Piping and instrumentation diagram (P&ID) of the autothermal reforming unit for oxygen-added conversion of Biogas to SynGas. (1) Gas-dosing lines for synthetic biogas and oxygen. (2) Biogas-gas pump. (3) Siloxane Filter. (4) Activated Carbon Filter. (5) Reforming Reactor with radial oxygen injection. (6) Combined heat exchanger for water evaporation and biogas preheating. (7) Feed water demineralization unit. (8) Feed water dosing pump.

reactants were fed into the reformer pre-chamber where O_2 was dosed through a radial injection system, ensuring thorough mixing of the input gases before entering the catalytic reforming stage. The combustible gas mixture was then fed into the catalytic reformer chamber for production of a CO_2-rich SynGas. A noble metal-washcoated monolith 0.7 l carrier catalyst was used for effective conversion of Biogas to SynGas (Interkat, Germany). The reformer was insulated using a machined microporous mantle, encasing the tubular gas mixing stage as well as the subsequent catalyst housing. The hot SynGas was passed into the HEX 950 for vaporization of feed water and preheating of the reactant biogas stream, supplying enough energy for feed overheating and maintaining stable reactor temperatures throughout, making the system truly autothermal, both concerning steady-state reactor operation and overall system energy balance. Additional heating was only required during the initial system start-up. Reformate was then fed through a cooled condenser, separating product water from the gas stream. SynGas was then run through a three-way valve, allowing for direct injection of the Gas into the MeOH-Process or separate operation of ATR and MeOH-synthesis in single-system investigation or for system start-up. The reforming system is illustrated in detail in Fig. 1.

2.2 Design and setup of the methanol synthesis system

For the effective conversion of SynGas with varying compositions, a MeOH-synthesis unit with a set of tubular reactors is applied. A P&ID of the integrated MeOH-synthesis system is given in Fig. 2. SynGas from the ATR unit is supplied to a gas mixing line through a three-way valve, which allows for individual system start-up as well as separate operation of the ATR unit and the MeOH-synthesis system. Here, H_2, CO and CO_2 can be dosed through thermal mass flow controllers (MFC – Bronkhorst EL-FLOW Select), which enables maximum composition control during system start-up and individual testing of the MeOH-synthesis loop. For the intended large-scale application of the herein presented system, H_2 from water electrolysis will be supplied to the SynGas for adaption of SynGas stoichiometry here. For small-scale pilot application, this was represented by dosing H_2 from gas cylinder bundles to specification.

The mixed gas is then compressed in a three-stage piston compressor (HAUG WTEGX 60/35/20) up to 25 bar system pressure. System pressure is limited due to guidelines related to the Pressure Equipment Directive of the European Union (2014/68/EU [PED]) based upon overall system gas volume and subsequent material testing requirements.[46] The compressed and H_2-added SynGas is then fed to a gas mixer and pulsation dampener, where it is mixed with the recycled SynGas and gas
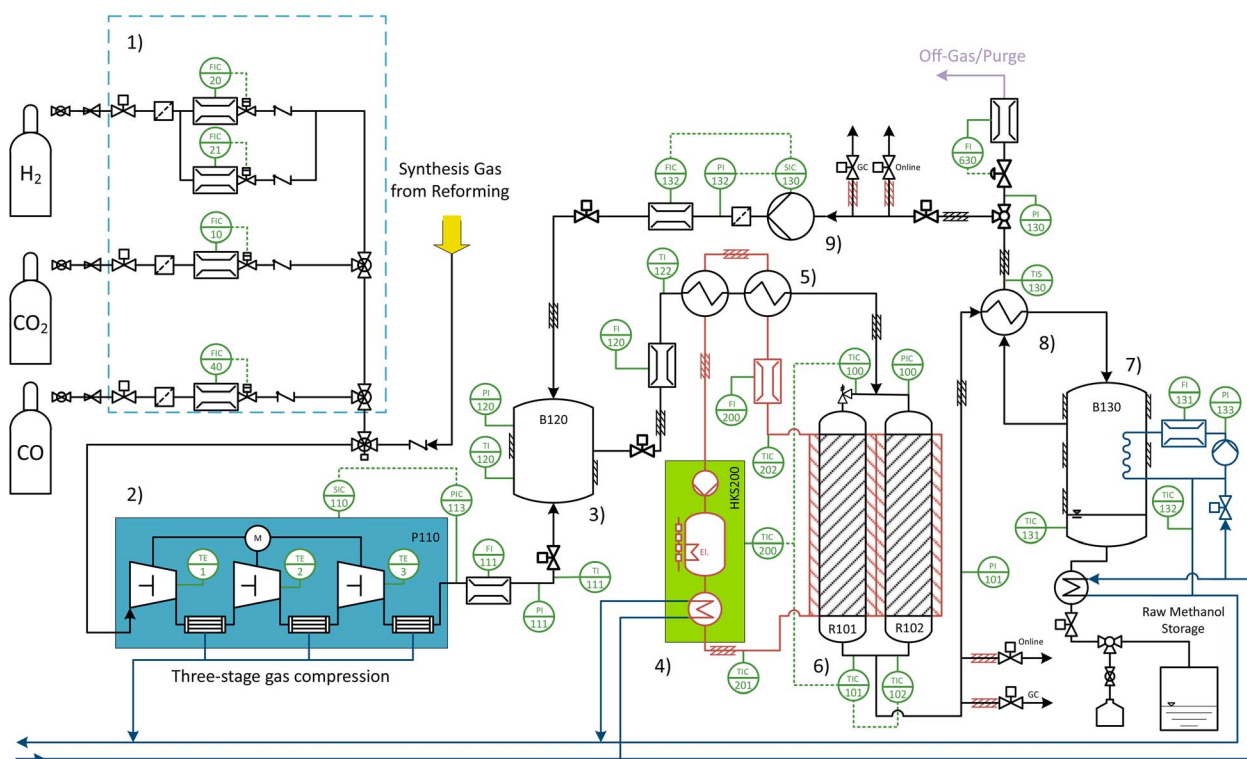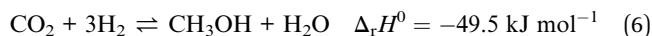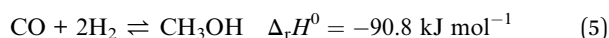

Fig. 2 P&ID of the methanol-synthesis loop for conversion of reformate from autothermal reforming. (1) Gas dosing lines for synthesis gas dosing from gas cylinders. (2) Three-stage synthesis gas compressor with intermediate stage cooling and condensation. (3) Gas mixer, combined heat exchanger and pulsation dampener for synthesis gas. (4) Thermal oil thermostat for system tempering during start-up and reactor cooling in steady-state operation. (5) Double heat-exchanger arrangement for synthesis gas pre-conditioning. (6) Double tubular quasi-isothermal methanol reactors. (7) Combined raw-product condensation and recycling gas conditioning unit. (8) Heat exchanger for product-gas cooling/recycling gas pre-heating. (9) Recycling gas compressor.

pressure and flow oscillations from the piston compression are smoothened. The SynGas-mixture is then fed through two heat exchangers arranged in series for preheating before entering the parallel tubular reactors. The reactors are stainless steel reactors with a 54.5 mm inner reactor diameter (ID) and 88.9 mm outer diameter (AD) including the stainless steel cooling/heating-jacket. The active reactor length is 1250 mm with a total reactor length of 1650 mm including flanges. The reactors were equipped with a metal grid base plate for support of the bulk catalyst filling. 2.048 kg of catalyst were applied to each reactor with the top and bottom headroom in the reactors being filled with glass wool for gas dispersion and particle filtering. As an MeOH-catalyst, a previously reported novel infiltration composite carrier catalyst coated with CuO, ZnO, CeO_2, ZrO_2 and CaO is applied.[47] Catalyst spheres had a diameter of 2.5 mm. SynGas is converted to MeOH and H_2O, with some of the entering CO_2 being converted to H_2O and CO through RWGS (cf. eqn (3)). Three general reactions take place in converting SynGas to the MeOH product, with several additional reactions yielding commonly reported byproducts such as dimethyl ether (DME), ethanol (EtOH), formaldehyde or methane not considered or analytically recorded in this work:[48]

$$CO + 2H_2 \rightleftharpoons CH_3OH \quad \Delta_r H^0 = -90.8 \text{ kJ mol}^{-1} \tag{5}$$

$$CO_2 + 3H_2 \rightleftharpoons CH_3OH + H_2O \quad \Delta_r H^0 = -49.5 \text{ kJ mol}^{-1} \tag{6}$$

$$CO_2 + 2H_2 \rightleftharpoons CO + H_2O \quad \Delta_r H^0 = 41.2 \text{ kJ mol}^{-1} \tag{7}$$

The oversaturated product gas is collected from the MeOH-reactors and fed into a stainless steel product condensation unit. Here, it is cooled through a counter-current gas heat exchanger (CC-HEX) and then fed to a water-cooled condenser, where liquid product is collected. Uncondensed SynGas is then fed back through the CC-HEX and fed back into the synthesis system through a high pressure recycling pump (Fink CHEM + TEC Z04-13). From there, the recycle gas stream enters the gas

mixer/pulsation dampener. A detailed illustration of the liquid product condenser is given in Fig. 2.

System pressure and off-gas flow were controlled through a high-precision proportional membrane valve (Samson EB 8091). Off-gas was taken from the recycling stream in front of the recycling pump.

The MeOH-synthesis system was managed thermally through a thermostat system (Huber Unistat TR401 wHT) with up to 8 kW heating and 10 kW cooling performance. Reactors were cooled through countercurrent perfusion of the tubular MeOH-reactors. Regenerated heat from reactor cooling was used for SynGas preheating in the serial HEX arrangement.

2.3 Integrated system and system control

The integrated system was set up in a 20 ft container with initial activated carbon treatment for sewage gas, raw MeOH-product collection and gas supply from gas cylinder bundles being housed in separate vessels. System control and operation was carried out from a second container with the overall decentralized pilot plant operation being conducted on site of the Emschergenossenschafts technical center on the WWTP Emschermündung in Dinslaken, Germany. The compositions of dry raw sewage gas, SynGas, MeOH product gas, and MeOH recycle gas were measured using an integrated gas analysis tower using two Rosemount X-Stream (Emerson, USA) Continuous Gas Analyzer systems with different infrared (IR) channels for CO, CH_4 and CO_2 analysis and additional thermal conductivity (TCD) channels for H_2-analysis. Gas streams for analysis were additionally fed to a multi entry port valve for sequential analysis in a GC unit (SRI Instruments 8610C) equipped with serial columns (9′ and 6′ Hayesep D). Liquid samples of the raw MeOH-product were analyzed for their composition ex situ on a HPLC unit (Shimadzu LCMS-2020). Samples were taken intermittently, usually for 20-minute test durations and weighed for determination of production rates.
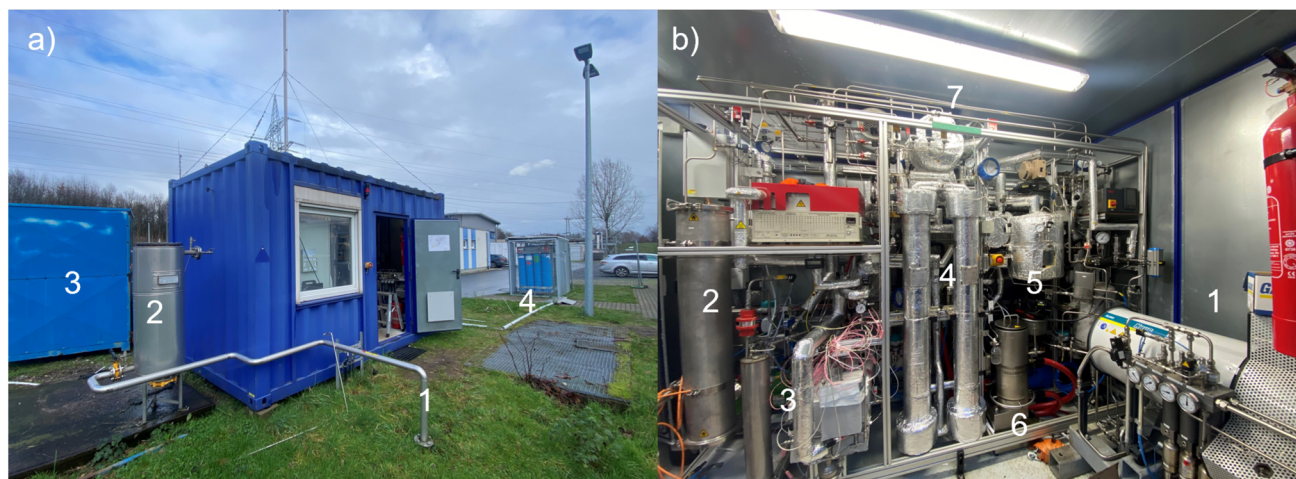
Fig. 3 (a) Outside view of the plant in operation. (1) – Sewage gas line. (2) – Activated charcoal filter. (3) – Gas storage for helium and calibration gas (GC). (4) – Gas storage for O_2, H_2, CO_2 and CH_4. (b) Inside view of the operational process. (1) – Three-stage reformate compressor. (2) – Siloxane filter. (3) – Reforming unit encased in a mantle. (4) – Tubular MeOH-reactors. (5) – Gas mixer/pulsation dampener. (6) – Thermostat heating and cooling unit. (7) – Heat exchanger for SynGas-preheating and energy recuperation.

The system was controlled through a custom Siemens Siematic programmable logic controller and a Windows Control Center (WinCC) user interface (Fig. 3).

3 Experimental

3.1 System parameters and performance indicators

3.1.1 Autothermal reforming. The ATR-process is governed by several key operating parameters that enable precise system control. The gas hourly space velocity (GHSV), defined as the normalized gas flow rate per unit catalyst bed volume, serves as a fundamental parameter for characterizing overall throughput in the ATR unit (eqn (8)). During pilot-scale operation, GHSV is regulated *via* controlled introduction of biogas, O_2, and water vapor into the reformer prechamber. Both the reforming temperature and the methane conversion efficiency are modulated by strategic oxygen dosing within the reforming unit. The stoichiometric relationship between oxygen and methane in the overall process is quantified by the air-fuel ratio (λ), where $\lambda = 1$ denotes the stoichiometric oxygen requirement for complete combustion of CH_4 to CO_2 and H_2O.

The intensity of steam methane reforming in the catalytic bed of the ATR unit (eqn (1)) as well as soot production and reforming temperature are controlled through H_2O supply.[49] The steam-to-carbon-ratio (S/C) is applied for process characterization and control, describing the ratio between dosed CH_4 and H_2O steam.

$$\text{GHSV} = \frac{\dot{V}_{\text{Gas}}\left(\text{Nm}^3\ \text{h}^{-1}\right)}{V_{\text{Catalyst}}(\text{m}^3)} \tag{8}$$

$$\lambda = \frac{\dot{n}_{O_2}}{2\dot{n}_{CH_4}} \tag{9}$$

$$\text{S/C} = \frac{\dot{n}_{H_2O}}{\dot{n}_{CH_4} + \dot{n}_{CO_2}} \tag{10}$$

Performance of the ATR is primarily characterized by H_2-content in the produced SynGas. For characterization of the dried SynGas, the stoichiometric number (SN) for MeOH-synthesis is applied. A sub-objective of the study is to minimize the necessary external H_2-injection for MeOH-synthesis, the measure of the stoichiometric conditions in dried SynGas or rather the lack thereof can easily be used for a review of the ATR performance. As conversion of CO to MeOH requires less H_2 and CO-content in produced SynGas is one measure of conversion-routes inside the ATR unit, the resulting carbon-oxide-ratio (COR) is used as an additional measure for ATR-performance as well as characterization and control of the MeOH-synthesis loop. It also represents an important measure for MeOH-system design, with conversion efficiencies and reactor sizing being heavily dependent on the ratio of injected CO and CO_2.[31]

$$\text{SN} = \frac{\dot{n}_{H_2} - \dot{n}_{CO_2}}{\dot{n}_{CO_2} + \dot{n}_{CO}} \tag{11}$$

$$\text{COR} = \frac{x_{CO_2}}{x_{CO_2} + x_{CO}} \tag{12}$$

3.1.2 Methanol synthesis. In a comparable manner to the ATR, MeOH-synthesis is strongly characterized by the GHSV through the MeOH-reactor (eqn (8)). In contrast to the reforming unit, gas velocity is a compounded value, made up of the gas velocity through the gas recycling section and volumetric feed rate of the reformate compressor. For both streams, the normalized volumetric gas flow rate has to be determined from gas analysis and mass flow detection. As moderate temperatures and low synthesis pressures are applied in this study, ideal gas conditions are assumed for normalization of gas flow rates into the reactor. SynGas dosing and recycle ratio in the SynGas recycling loop are regulated towards high GHSV of 7000 h^{-1} and above, which is a common parameter range in commercial MeOH-synthesis.[50] In system analysis, the ratio between input SynGas stream and recycling gas stream pumped through the recycling gas loop is calculated as the recycling ratio, which describes the molar fraction of recycled gas over reformate.

Hydrogen is dosed based upon the SN-value of reformate delivered through the compressor. A minimum of SN = 2 is applied for stoichiometric SynGas composition for carbon-oxide conversion to MeOH and H_2O. For each steady state operation point of MeOH synthesis, an additional, real SN can be derived, which combines SN from reformate dosing and SN in the recycle loop of the synthesis system.

$$r_{\text{recy}} = \frac{\sum \dot{n}_{\text{recy},i}}{\sum \dot{n}_{\text{reformate}_i}} \tag{13}$$

For determination of conversion performance inside the MeOH-reactor, two different measures of conversion can be applied: single-pass reactor conversion ($X_{C_{sp}}$) is used to characterize the catalyst performance, representing the catalyst's ability to convert carbon-oxides to liquid process products in a single reactor pass. This performance metric was monitored continuously. It was calculated as the difference in molar CO- and CO_2-flux in the reactor inlet and the molar streams being recycled and purged respectively. The formation of by-products, such as dimethyl ether (DME), Formaldehyde (FAD) or CH_4, which are commonly generated alongside MeOH in low pressure synthesis, is disregarded for this analysis.[51–53]

A second performance indicator is the overall system carbon conversion ($X_{C_{tot}}$). It represents a balanced value, indicating the amount of carbon converted to MeOH-product over a defined time frame in testing. This is also used as an overall system performance measure, as all carbon-reactants used in ATR are subsequently fed into the low pressure MeOH-synthesis system as ATR products.

$$X_{C_{sp}} = 1 - \frac{\dot{n}_{CO_2,\text{recy}} + \dot{n}_{CO_2,\text{purge}} + \dot{n}_{CO,\text{recy}} + \dot{n}_{CO,\text{purge}}}{\dot{n}_{CO_2,\text{in}} + \dot{n}_{CO,\text{in}}} \tag{14}$$

$$X_{C_{tot}} = \frac{n_{\text{MeOH}_{tot}}}{n_{CO_2,\text{in,tot}} + n_{CO,\text{in,tot}}} \tag{15}$$

For determination of overall system efficiency, the chemical efficiency was used, which can be calculated by determining the heating value (HHV) of the molar input streams, output streams and other associated process streams.

$$\eta_{ch} = \frac{\sum \dot{n}_{i,product} HHV_{i,prod}}{\sum \dot{n}_{i,in} HHV_{i,in}} \quad (16)$$

As both O_2 and H_2 are injected into different parts of the two-stage thermochemical process in combined system operation, a performance review of the use of both products of electrolysis was performed based upon the relation between injection requirements in O_2 addition for ATR and H_2 addition for stoichiometric MeOH-synthesis. The relation between the gas injection requirements is given as a percentage of stoichiometric gas production in electrolysis, with 100% denoting injection requirements exactly proportional to electrolysis gas production (two parts molar H_2 to one part O_2), with values larger than 100% denoting excessive hydrogen demand and values lower than 100% denoting excessive oxygen demand for the respective system set point:

$$\eta_{electrolysis} = \frac{\dot{n}_{demand,H_2}}{\dot{n}_{demand,O_2} \times 2} \times 100 \quad (17)$$

In a comparable manner, the relationship between H_2 produced from biogas and H_2 required from electrolysis for stoichiometric SynGas injection into the MeOH-synthesis system (SN = 2) can be described as

$$\phi_{H_2} = \frac{\dot{n}_{H_2,el}}{\dot{n}_{H_2,ATR}} \quad (18)$$

with values larger than 1 indicating more hydrogen in the system being supplied through the electrolysis unit and values lower 1 indicating hydrogen supply weighted towards ATR reformate.

3.2 System start-up and determination of steady-state

3.2.1 Autothermal reforming. Startup of the ATR unit requires heat-up of the combined heat exchanger and the reforming reactor itself. The energy required to temper the system is supplied through electrical trace heating of the system. During system heat-up, N_2 is fed through the system for inertization. The heat supplied to the system before autothermal operation is defined by the energy requirement for full evaporation of the dosed H_2O-stream and the minimal heat required for the ignition of the partial CH_4-oxidation reaction, which has been reported to be around 230–400 °C – depending on the applied catalyst structures.[54,55] 400 °C was chosen as target temperature set point for reformer start-up in the piloting of the described plant. When both the reforming reactor and the combined heat exchanger reached the necessary temperatures for catalyzed CH_4-oxidation and total vaporization of the H_2O-feed, H_2O was dosed into the system. Biogas-injection was started as soon as the vapor stream reached the inlet of the

reforming reactor, which was indicated reliably by a temperature drop at the reactor inlet – with temperatures being continuously monitored throughout operation of the reformer. Cascaded feed injection during reactor start-up was necessary to avoid soot formation and keep the reactor in its defined operating window, as is common in industrial full-scale reformer operation.[56] As H_2O vapor and biogas mix at the catalyst inlet, the endothermic steam reforming reaction (eqn (1)) is triggered, which leads to a second temperature drop at the reformer catalyst inlet. At this point, O_2-injection was triggered and λ was increased until a stable operating temperature was reached under constant biogas load and H_2O injection rates. For system equilibration the ATR unit was operated at low operating loads until stable steady state operation at $\lambda < 0.3$ and S/C = 1.3 was recorded. After system equilibration, a different set-point for ATR operation was chosen and applied for system testing. Gas compositions for biogas entering the reforming unit and for dried SynGas were monitored online with S/C and λ both being calculated through the measured biogas input feed and its composition. Produced SynGas was purged during system start-up.

3.2.2 Methanol synthesis. For the start-up of the MeOH-synthesis system, the system was pressurized with pure H_2, with the purge gas valve closed and the recycling gas pump set to achieve a GHSV of around 5000 h^{-1}. During pressurization, the reactors and SynGas heat exchanger were heated using a thermostat (HKS200 – Fig. 2). After reaching the desired system pressure, the compressor (P110 – Fig. 2) was shut off and H_2 was recycled through the system until temperature equilibration of the system was reached. After temperature equilibration in the closed H_2-synthesis loop, injection of SynGas was started (compare Fig. 4). In MeOH-synthesis-only operation, a SynGas-set point was chosen and CO- and CO_2-injection was controlled to achieve a constant SynGas stream with 3 > SN > 2 and COR of 0.5–1.0. P110 was then re-engaged for constant SynGas-feed into the system.

In combined operation, P110 was engaged and the 3-way valve separating the reforming unit and MeOH-synthesis system was switched to allow for SynGas pumping into the MeOH-synthesis system. Gas composition was monitored after P110, after reactor pass or in the recycling gas loop prior to pumping towards the gas mixer. To achieve a certain SN, H_2 is dosed according to the composition of SynGas before entering the gas mixer (B120 – Fig. 2).

This guaranteed optimal composition of feed SynGas but in turn led to suboptimal SynGas compositions in recycling gas or in mixed SynGas prior to entering the reactors, which could be counteracted upon through superstoichiometric H_2-dosing towards higher SynGas SN.

4 Results

4.1 Combined operation of ATR and MeOH-synthesis

For combined operation of the two subsystems, a system start-up according to the aforementioned protocols is carried out for each of the processes. Herein, the MeOH-synthesis system is pressurized using pure H_2 as a medium, thus also guaranteeing
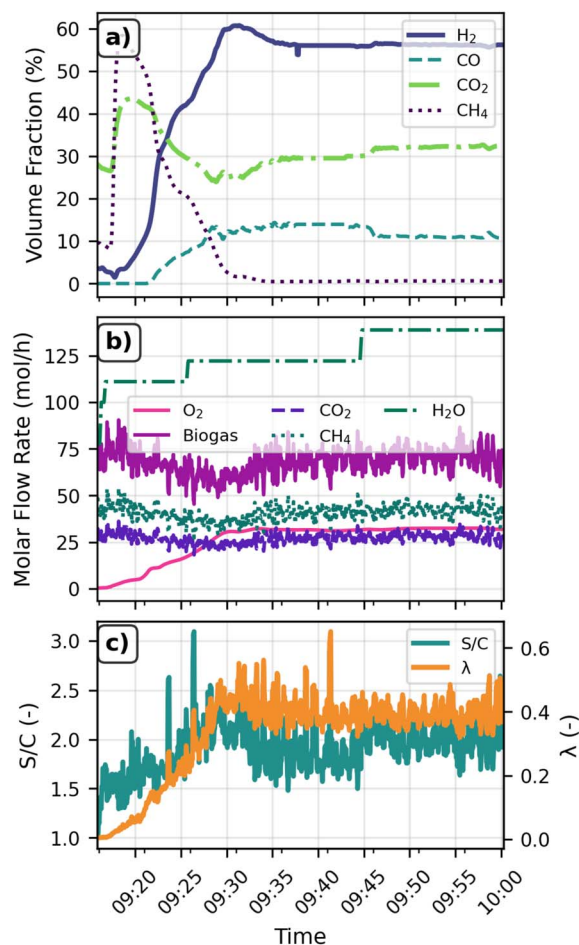
Fig. 4 Reformer start-up after preheating of the catalytic chamber and the combined heat exchanger and start of O_2-injection for autothermal operation. (a) Reformate composition after reformer start-up. Steady-state gas composition is reached after 10 minutes. (b) Record of feed injection into the reformer for the depicted start-up procedure. (c) λ and S/C for the presented start-up protocol.

full reduction of the applied catalysts before combined SynGas-operation. The separated operation of ATR and MeOH-synthesis is ensured by a 3-way valve. Once equilibrated system operation at low load for ATR and H_2-only synthesis loop pressurization for MeOH-synthesis are reached, the valve is switched and P110 engaged to allow for SynGas compression into the MeOH-synthesis.

4.2 System start-up

System start-up of the ATR unit was comparatively straightforward in standalone operation. Reformate composition was controllable directly through H_2O injection and adaption of λ, CO-content of the raw SynGas was directly correlated to O_2-injection. Fig. 4 shows gas compositions in the reformer exit SynGas for dosing ramp-up of O_2 and H_2O-vapor for a setpoint at 2.0 kg h^{-1} (2.4 m^3 h^{-1} – 68% system load). The recorded time represents actual day-time of the presented start-up protocol – the start-up procedure was started at 9:20 am, steady-state reformate conditions were reached 10 minutes later. As can

be observed, CH_4 and CO_2-content of the reformer effluent reflect the composition of raw biogas at the beginning of the start-up procedure. Increased λ leads to a gradual decrease of residual CH_4 down to near total oxidation 15 minutes into the reformer start-up. The system reaches a steady state at $\lambda = 0.3$ and S/C = 1.8 after 25 minutes. A slight increase of S/C at 09:45 is clearly reflected in a slight change of reformer effluent COR, with CO dipping by about 3 percentage points through the increase in vapor injection. Equilibration of the reformer system is reached only a few minutes after the change in S/C.

4.3 Operation of the biogas ATR

For identification of optimal ATR operational parameter set points, a series of tests was carried out using different S/C, λ and GHSV. Biogas composition in the test runs reported on was approximately $60\%_{vol}$ CH_4 and $40\%_{vol}$ CO_2. Nominal capacity of the reforming unit and subsequently for the entire Bio–MeOH synthesis plant was reached at 3.5 m^3 per h biogas. This translated to a space velocity of approximately 15000 h^{-1} applying λ of 0.3 and S/C of 1.3. Depending on S/C, λ had to be set to 0.2 to 0.45 to achieve truly autothermal reforming conditions, with H_2O-evaporation consuming significant amounts of the heat generated through partial CH_4-oxidation. In ATR-only tests, S/C was set at 1.3. This ensured the minimization of soot production with H_2O injection inhibiting the production of soot through carbonization.[57] Overall biogas feed and λ were set accordingly to achieve autothermal conditions and operational optimization was directed towards the optimization of COR and SN in the SynGas produced, with high SN and low COR being generally favorable for effective SynGas conversion toward MeOH over $CuO/ZnO/Al_2O_3$-based catalysts.[58] Fig. 5 depicts the steady state results for the pilot ATR unit at S/C = 1.3 for varying λ and GHSV. At constant GHSV, increasing λ leads to expected higher temperatures inside the catalytic reaction chamber of the reformer as more CH_4 is oxidized. Increased feed rates and subsequent higher GHSV also lead to an increase in reaction temperature as the overall molar catalytic turnover is increased to yield higher reforming temperatures. Through change in GHSV, the load setpoint of the plant is controlled and different GHSV at set λ and S/C slightly influence the performance of the reforming unit with changing gas residence times in the catalytic reactor. An increase in GHSV at constant λ and S/C led to increased CH_4-conversion to CO, benefiting the resulting SynGas COR and SN with H_2-content in the reformate not being affected much by the reduction of gas residence time. This is in line with previous reports in autothermal and steam-methane biogas reforming.[59] At nominal load, the highest H_2-content and highest SN are reached at $\lambda = 0.25$, although CO_2-contents are significantly higher at low λ. This is attributed to the fact that CO_2-content does not change much at all over changing λ, implying that most of the CO_2-content observed in the SynGas actually stems directly from the biogas input, not being converted but passing through the reformer inertly. The CO-content however significantly changes with increasing λ, indicating partial oxidation and contributing to COR and SN through enhancing CO-
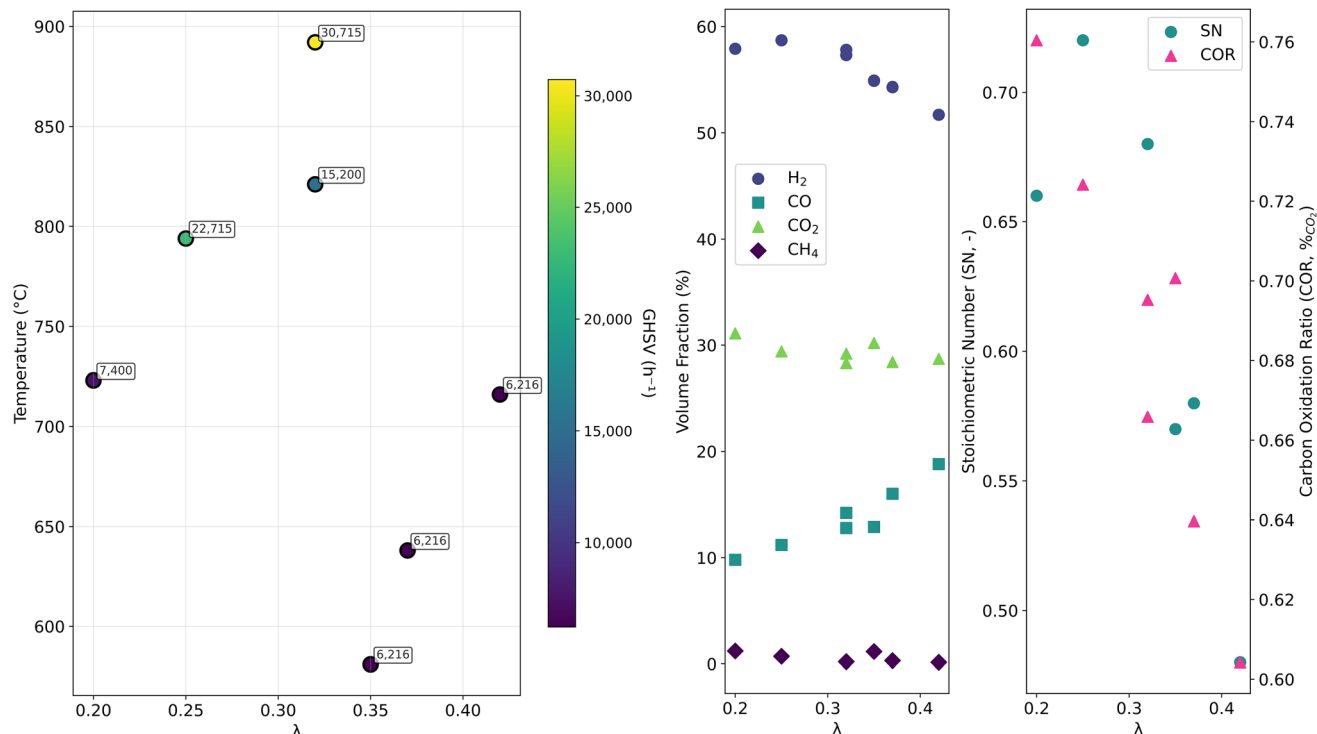
Fig. 5 Operational results for separate ATR–operation under different GHSV and λ at S/C = 1.3.

content in the SynGas. Fig. 6 shows calculated ϕ and η_{el} for the previously mentioned λ tested in ATR-only operation. As can be deduced from the figure $\lambda = 0.25$ generates SynGas with the highest H_2-content, leading to the lowest additional theoretical H_2-injection into the coupled MeOH-synthesis system. At the same time, increased λ leads to less favorable COR and higher

additional H_2-demands in the MeOH-synthesis process. In industrial application this would lead to a higher demand for installed electrolysis power but to a more equalized consumption of pure H_2 and O_2 from the coupled electrolysis unit. Overall this shows that lower λ values lead to more favorable conditions for SynGas-conversion to MeOH, also reducing pure O_2-demand in large scale application of the technology in combination with electrolysis.
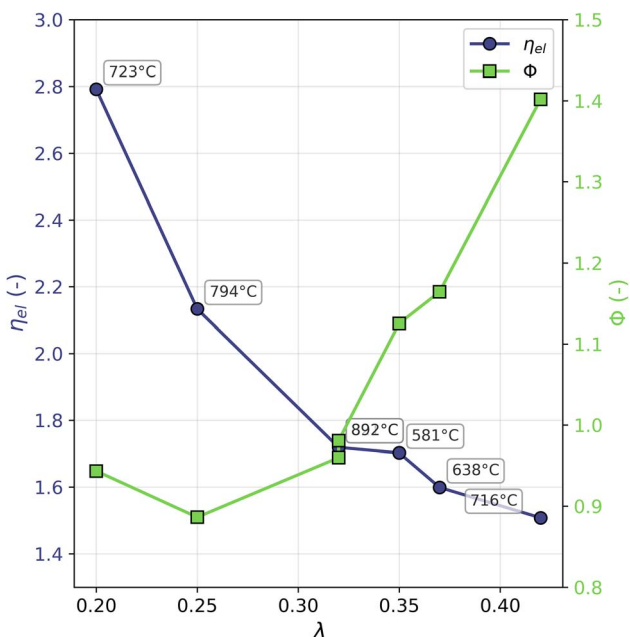
4.4 Operation of the MeOH-synthesis loop

4.4.1 System start-up and equilibration. As single-pass conversion ratios inside the MeOH-reactors are usually considerably lower than 50%, high portions of the SynGas fed to the reactors stem from gas recycling through the recycling loop.[60] A steady-state reaction state is only reached once the state inside the loop, or alternatively at the reactor inlet has balanced out to a constant gas composition, constant temperature and constant feed rate. For investigation of the steady-state gas compositions reached in MeOH-synthesis from reformed biogas, different reformate mixtures were tested towards their respective subsequent steady-state reaction compositions. Fig. 7 shows the start-up composition development in the SynGas recycling loop for four different input gas compositions. The input gas COR dosed into the system through the compressor is given for each plot. All test compositions were tested at SN = 3. As can be deduced from the figure, mixed carbon-oxide gas compositions set in for all tested input gas COR. Even in pure CO_2-dosing (COR = 1), a recycle loop COR of 0.63 is reached after equilibration of system gas

Fig. 6 Φ and η_{el} of the different tested operational setpoints for the ATR.
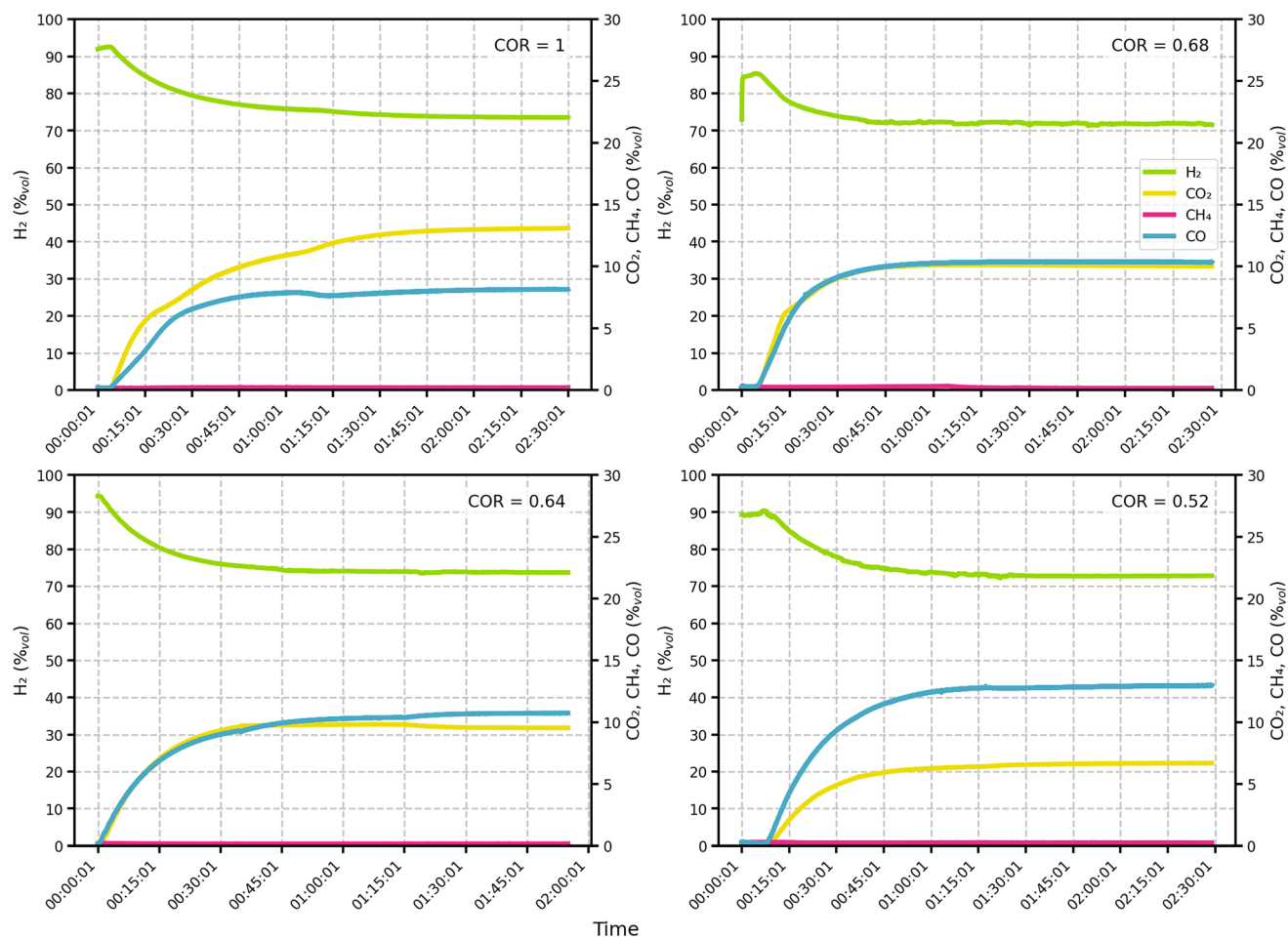
Fig. 7 Recycle loop gas composition after system start-up ($t = 0:00$) of the methanol synthesis unit. Depicted COR reflects the COR of injected SynGas into the system over the period of system start-up and equilibration. Times used in x-axes refer to test duration from the beginning of the recording.

compositions. This highlights the importance of mixed carbon-oxide testing in catalyst development, as overall gas compositions in synthesis loops will always contain some amount of CO produced through RWGS. Dosing of SynGas compositions of COR around 0.64–0.68 leads to near equalization of the carbon-oxide content in the recycling gas stream, with both CO- and CO_2-content evening out at $10.5\%_{vol}$. The system equalization was usually reached approximately 2 hours after the change in the setpoint of the system, with the CO_2-only SynGas dosing facilitating the longest equalization times after the change of the system setpoint. This has important implications for the dynamic operation of future E–MeOH and Bio–MeOH process plants, as system setpoint or load changes do not reflect in the recycling gas composition quickly.

4.4.2 Steady state operation results. The MeOH-synthesis unit was tested for conversion efficiency, equilibrium system gas compositions and methanol yields with several different input SynGas streams. In MeOH-only operation, these compositions were taken from equilibrium calculations for the ATR, yielding four probable SynGas compositions concerning COR and an additional test condition for COR = 1, dosing only CO_2

and H_2, representing E–MeOH operation of the system, where pure CO_2 would be dosed from an upstream carbon-capture process such as membrane CO_2-capture or amine-washing-applications.[61] As SynGas was not expected to deliver stoichiometric H_2-contents, SN was not considered as a factor in choosing applicable ATR-conditions for the MeOH-system-only operation runs. For each of the calculated COR, SN could be set to stoichiometric or superstoichiometric conditions through pure H_2 injection. As system pressure was limited to 20 bar, conversion ratios were expected to be low compared to industrial applications on the basis of previous laboratory results for the catalyst sample applied in this work.[47] Therefore, the investigation presented herein concentrates on the influence of SynGas COR, reactor temperatures, and SN on the synthesis performance in MeOH synthesis as well as the resulting conditions in mixed SynGas streams. Increasing the reaction pressure will significantly impact equilibrium reaction conditions over the catalyst and leads to significantly improved $X_{C_{sp}}$ in steady-state system operation, with some studies showing a two-fold increase in MeOH-yield over an two-fold increase of reaction pressure, depending on GHSV and reaction
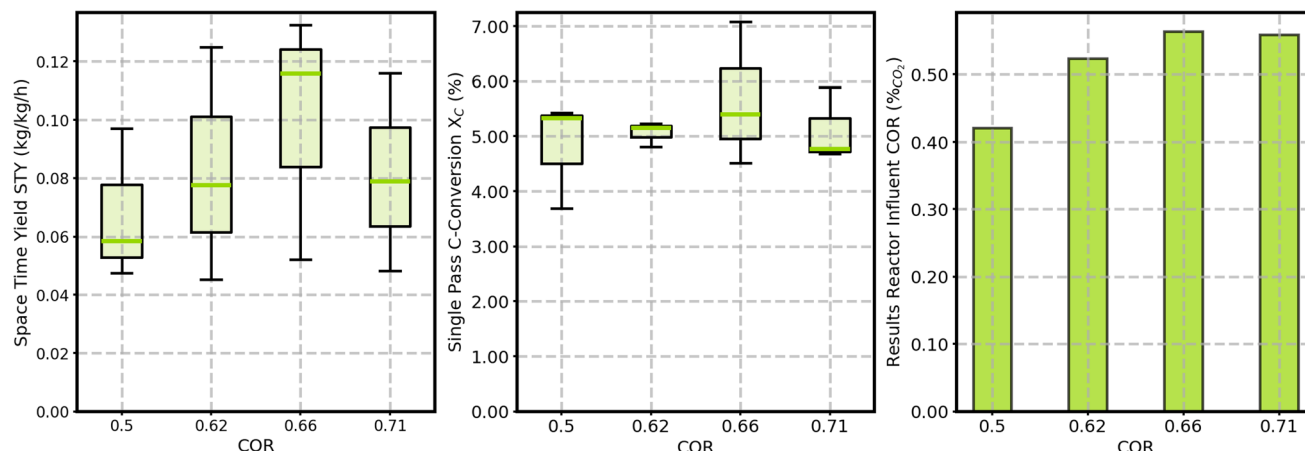
Fig. 8 MeOH-unit STY, $X_{C_{sp}}$ and resulting reactor influent COR for four different SynGas COR used in separate MeOH-testing.

temperatures.[62,63] Fig. 8 depicts different STY, $X_{C_{sp}}$ and resulting steady state reactor influent COR, calculated from SynGas COR and recycling gas COR with corresponding mass flow rates. Tests with COR 0.66 COR reformate influent show the highest overall STY and $X_{C_{sp}}$ at 250 °C and 20 bar reactor pressure and also lead to the highest SynGas COR during steady-state operation reactor entry. This can most likely be attributed to the composition being close to the steady-state synthesis gas composition in MeOH-synthesis over the herein tested quinary carrier catalyst. Through this, CO_2 is converted less readily to CO through RWGS, making it available for MeOH generation with less of the otherwise produced CO being purged from the system in system pressure regulation. This is shown in the rightmost plot for reactor influent COR, where the average COR calculated at the reactor entry is closest to raw SynGas COR at 66%. Additionally, the herein measured 0.11 g_{MeOH} per $g_{Catalyst}$ per h STY_{MeOH} quite accurately reproduces formation rates previously reported for the catalyst at 20 bar reaction pressures and comparable SynGas COR.[47] GHSV has a profound effect on MeOH-generation. In laboratory set-ups, GHSV can be controlled independently of other system parameters. In pilot operation, this control is not applicable, as GSHV is directly correlated to conversion and purge ratios, which in turn are directly correlated to temperature, COR, SN and GSHV again. An overview on GHSV's influence on STY_{MeOH} is given in the SI files. In E–MeOH-operation (COR = 1), the reactor temperature has a major influence on the conversion results, as RWGS is greatly influenced by it. High temperatures facilitate higher rates for the reverse shift, resulting in a significantly lower COR in the synthesis loop and an overall shift towards H_2O production.[64,65] As is expected and as is shown in Fig. 9, high temperatures lead to the highest overall STY, but lead to a drop in system COR by 30 percentage points. Raw product composition is shifted from 45% MeOH content to 35% between 225 °C and 275 °C reactor temperatures with the overall production rates increasing nearly threefold over this temperature range. This again demonstrates the importance of mixed carbon-oxide conversion efficacy of future catalyst systems towards selective

conversion of CO_2 to MeOH and the inhibition of premature CO desorption in RWGS in renewable Bio– or E–MeOH-processes.

4.5 Combined system operation

4.5.1 Operational aspects of combined system start-up and operation. In large scale fossil MeOH-synthesis operation, start-up and shut down procedures are not commonly performed. In decentralized production of Bio–MeOH or E–MeOH, volatile plant operation according to external factors like electricity spot market price is more likely in the future and can impact operating costs or cost of production for MeOH.[66,67] Equally, operation with or without the reforming unit is possible, reacting to price changes for flexible plant operation. Likewise, small-scale and pilot plant operation facilitates more frequent start-up procedures taking into account safety measures and effective start-up times.
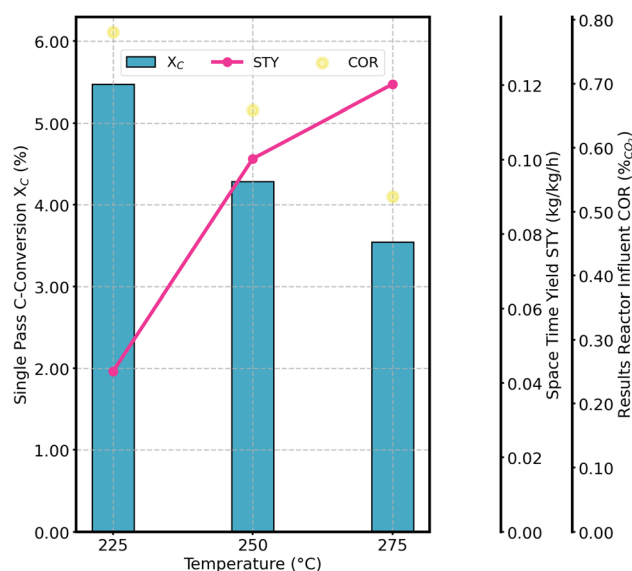

Fig. 9 MeOH-unit STY, $X_{C_{sp}}$ and resulting reactor influent COR in CO_2-only operation at different temperatures and SN = 2.

Species (-)	Stream 1 (mol/h)	Stream 2 (mol/h)	Stream 3a (mol/h)	Stream 3b (mol/h)	Stream 4 (mol/h)	Stream 5 (mol/h)	Stream 6 (mol/h)	Stream 7 (mol/h)	Stream 8 (mol/h)	Stream 9 (mol/h)
H_2		115,0	84,8	199,8	2686,1	2885,9	2791,2		105,3	2686,1
O_2		27,5								
CH_4	41,8		2,1	2,1	50,7	52,8	103,5		1,9	50,7
CO_2	27,9		46,3	46,3	517,1	563,4	534,2		20,3	517,1
CO			21,2	21,2	509,6	530,8	535,6		19,9	509,6
H_2O	111		97,2	10,3		10,3	45,7	45,7		
CH_3OH							24,3	24,3		

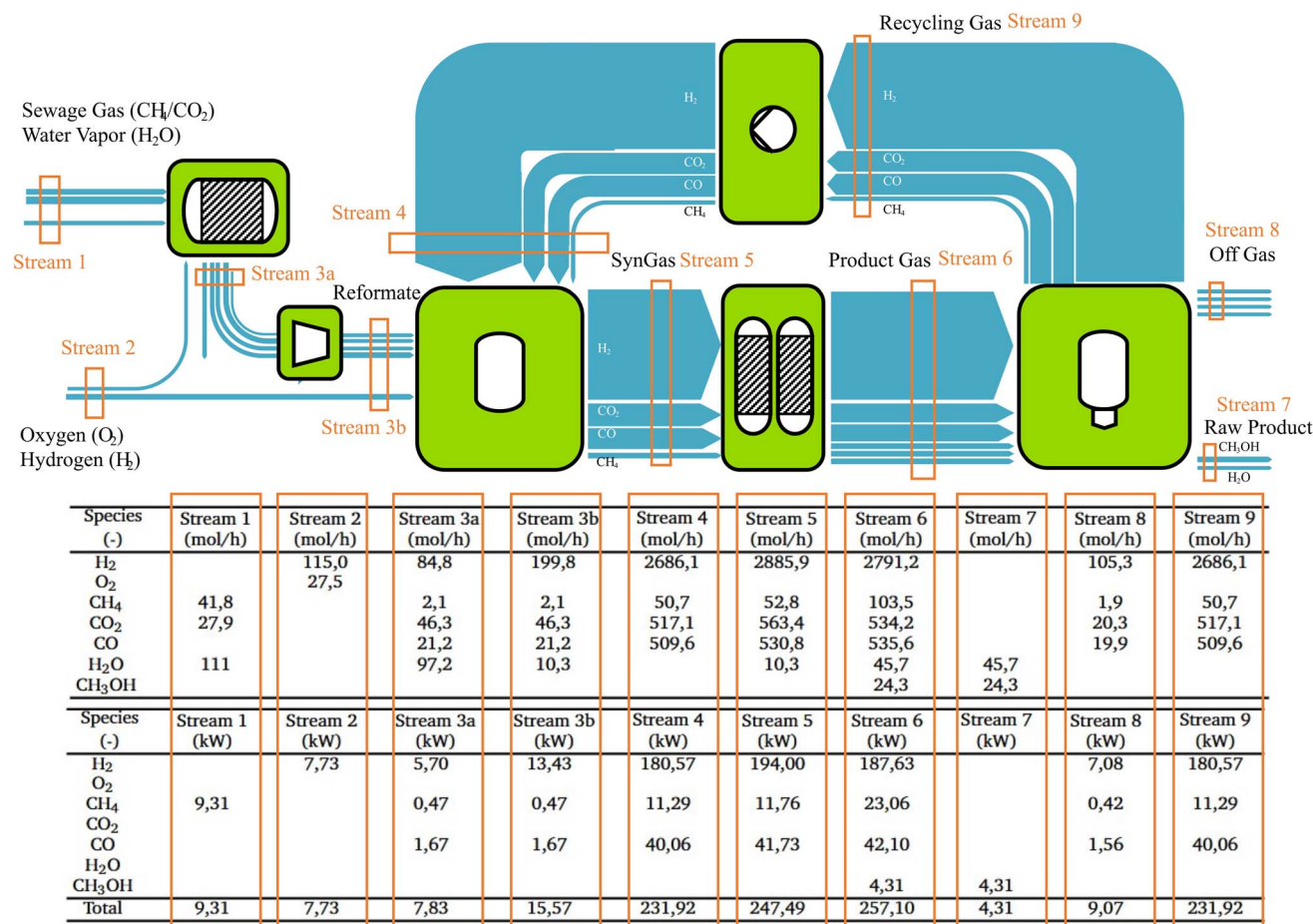| Species (-)	Stream 1 (kW)	Stream 2 (kW)	Stream 3a (kW)	Stream 3b (kW)	Stream 4 (kW)	Stream 5 (kW)	Stream 6 (kW)	Stream 7 (kW)	Stream 8 (kW)	Stream 9 (kW)
H_2		7,73	5,70	13,43	180,57	194,00	187,63		7,08	180,57
O_2										
CH_4	9,31		0,47	0,47	11,29	11,76	23,06		0,42	11,29
CO_2										
CO			1,67	1,67	40,06	41,73	42,10		1,56	40,06
H_2O										
CH_3OH							4,31	4,31		
Total	9,31	7,73	7,83	15,57	231,92	247,49	257,10	4,31	9,07	231,92

Fig. 10 Sankey diagram of the balanced steady state system for the combined operation of ATR and MeOH-synthesis with molar and energy flux given for each compounded process stream. Bar thickness correlates with molar flux.

Table 1 Performance data for combined operation series at moderate system loads

Load (%)	65	66	71	68	68
λ (—)	0.31	0.31	0.36	0.32	0.32
S/C (—)	1.39	1.36	1.49	1.58	1.42
COR_{Ref} (%)	0.72	0.65	0.62	0.67	0.66
SN_{Ref} (—)	0.61	0.58	0.62	0.57	0.58
$\eta_{electrolysis}$ (%)	187	191	160	184	185
COR_{Syn} (%)	0.57	0.51	0.49	0.51	0.53
MeOH STY (kg per kg_{cat} per h)	0.08	0.09	0.13	0.12	0.11
X_c (%)	31	36	39	37	35
MeOH (%wt)	33.6	37.2	39.4	38.5	38.0
H_2O (%wt)	66.4	62.8	60.6	61.5	62.0

For combined system operation, start-up procedures of the separate thermochemical systems were carried out following the aforementioned protocols. Once a steady-state was reached in both subsystems, they were connected, switching the three-way valve separating both subsystems from purge operation to combined operation. While in principle they are easily attainable, pressure gradients in the gas feed line between the reforming unit and compressor during the short moment of

system merging were observed repeatedly. These were most probably caused by a short reduction of reformer effluent flow rate while compressor entry pressures equalized. This short adjustment period led to a slightly increased retention time of the SynGas inside the ATR catalyst chamber. The reduced GHSV through the reforming unit in turn led to increased residence time and slightly intensified catalytic reaction rates of CH_4 and O_2 leading to short term temperature spikes, which led to automated system shut-off in system piloting on multiple occasions.[60]

Based upon these observations, a combined system start-up procedure was optimized operationally. For safety measures, both subsystems were operated at steady state, minimal load conditions, which were dictated by the minimal feed rate of the SynGas compressor, *ca.* 65%. Furthermore, λ was reduced to a minimum, guaranteeing a low GHSV through the reformer and inhibiting combustion that exceeds the set-point range limits of the reformer in system-merging. For future application, initial system start-up is advised to be carried out in merged process configuration to avoid the hydraulic disadvantages of valve switching between two steady-state processes. The possibilities of dynamic, economically optimized E–MeOH

operation of combined systems necessitate operationally robust procedures for merging.

In steady-state system operation the low conversion performance of the applied, prototype MeOH catalyst at the limited applicable system pressures resulted in a second operational obstacle: as SynGas was not converted to liquid product at the expected rates, more of the gas inside the MeOH-synthesis loop had to be recycled. For optimal overall performance, this led to the reduction of reformer load and the decreasing of compressor load and subsequent minimization of reformate fed into the pressurized MeOH-synthesis.

As the compressor was limited in is minimum load operation (65%), more SynGas was compressed into the system, as could be converted for system pressure equilibration. In turn, gas purging had to be increased to unusually high proportions, in order to attain steady-state combined operation set points which led to the emission of excessive amounts of unconverted carbon. In the overall system performance assessment, this led to poor total conversion ratios in combined system testing and reduced the amount of possible system set points. In future system optimization, system pressure will be increased and a modern commercial catalyst applied. For higher conversion ratios, this will increase the range of possible SynGas feed setpoints, reduce the amount purged off-gas and improve the ratio between recycled gas and injected reformate.

4.5.2 Results of combined system operation. For combined system operation, the system was operationally optimized towards minimization of off-gas purging and reformer operation stability, thus providing the basis for long-term steady state operation and maximizing overall SynGas conversion towards MeOH. In system testing, four stable operational set points were found, tested and optimized. Due to the overall low conversion at the aforementioned synthesis pressures, very high recycling ratios were applied to ensure maximum overall residence time of the injected carbon-oxide species in the MeOH-reactors. This led to high GHSV through the MeOH reactors, in turn impacting the system performance with higher GHSV having to be shown to increase MeOH-yield but reduce overall conversion ratios in mixed carbon-oxide SynGas streams.[68]

Fig. 10 depicts the calculated molar and energy flux inside the system for a typical steady-state set point utilizing $S/C = 1.58$ and $\lambda = 0.32$ in the ATR and adding H_2 to reach $SN = 2.25$. The molar flux was calculated using mass flow measurements inside the system and online gas composition measurements to determine the molar mass of the stream and the overall molar flux. Energy flux was calculated using the heating values (HHV) of the species in each molar stream depicted in the system. As can be deduced from the figure, the ratio between recycling gas stream (Stream 4) and reformate input stream (Stream 3b) is 14.46, exceeding industrial application standards three- to six-fold.[50] Concerning chemical efficiency of the system, an overall efficiency of 25.29% was reached for the steady state depicted in Fig. 10. As described in Subsection 4.4.1, this is due to the excessive amount of gas purging related to the minimal compressor set point for steady state operation. In the referenced steady state set point, approximately twice the energy flux

was purged through H_2- and CO-content of off-gas emitted from the synthesis.

Results for the five steady state system setpoints typically reached and optimized in combined system operation are given in Table 1. As reformate COR and SN did not widely vary across the different reached setpoints and system loads, dosed H_2 and overall equilibrium gas compositions in the MeOH synthesis loop did not change significantly as well. This is reflected accordingly in the recorded reformate COR and SN as well as MeOH synthesis loop COR, which are within 16% of each other when comparing the minimal and maximal set point values achieved in system testing. The highest STY_{MeOH} is reached at the highest stable system load, which was operationally achieved at approximately 71% compressor rotational speed, equal to 5 $Nm^3 h^{-1}$ of reformate injection into the system or around 3.2 kg h^{-1}.

5 Conclusion and outlook

In the herein presented work, we designed, commissioned and operated a pilot plant for producing MeOH from biogas through a complex system comprising an ATR and a MeOH synthesis loop, utilizing pure O_2 for operation of the ATR and pure H_2 for improving SynGas stoichiometry in MeOH-synthesis. The system is designed on a small but fully operational scale to represent a future system applying electrolysis for the supply of H_2 and O_2. We operate both thermochemical systems independently of each other, optimizing both subsystems towards efficient set-points independently of each other, testing the MeOH-synthesis loop additionally for its effectiveness in handling SynGas comprising pure CO_2 and H_2. Furthermore, we introduce an operational approach for coupled system start-up and stable operation. We identify several operational hurdles in system design and stable steady-state operation and propose strategies for overcoming the identified hurdles. Overall, the herein proposed system shows great potential towards future application in decentralized material usage of biomass of biogas, while several key obstacles prevail on the path to industrialized application of the biogas-to-MeOH process, both on a pilot-scale level as well as future industrial scale levels: on the tested pilot scale of the system, system-back pressure gradients in ATR and MeOH-synthesis coupling led to complications in λ-, S/C and subsequent temperature regulation in ATR. To tackle these complications, we propose a minimal load start-up operation set point to avoid temperature fluctuations in system coupling, thus laying the foundations for stable system start-up and future applications, where system load could be managed according to external factors such as electricity spot-market prices. In MeOH-synthesis, low applied system pressure and overall reduced activity of the novel tested catalyst lead to decreased conversion of both CO and CO_2 towards MeOH in the reactors. This in turn leads to excessive gas purging from the system, as minimal reformate feed is limited by the operational range of the compressor P110. This leads to suboptimal setpoints in the MeOH-synthesis loop, utilizing very high recycling ratios and subsequent GHSV through the parallel MeOH-reactors. Nonetheless, the presented work demonstrates the

possible potential of the system under further optimization. Similarly, theoretical studies have shown that minimizing the purge gas ratio and maximizing $X_{C_{sp}}$ by applying higher system pressures and utilizing MeOH-catalysts of industrial efficiency, the system should be able to achieve η_{ch} of 50–60% in the future.[11,15] Especially in Germany, where many decentralized biogas facilities are in need of value added alternatives to biogas applications as fuel for electricity and heat production, decentralized systems for material biogas conversion towards fuels of chemical substitutes can play a central role in defossilization of the otherwise fossil carbon reliant industries.

Author contributions

Carl Fritsch – conceptualization (MeOH-synthesis), data curation, formal analysis, funding acquisition, investigation, methodology, project administration, resources, supervision, validation, visualization, original draft. Jule Blankenstein – data curation, investigation, methodology, validation, review & editing. Benedikt Bender – conceptualization (ATR-reformer), data curation, formal analysis, funding, investigation, methodology, review & editing. Jürgen Dornseiffer – conceptualization, methodology, supervision, review & editing. Moritz Haep – investigation, data curation, formal analysis. Kristoffer Ooms – conceptualization, funding.

Conflicts of interest

There are no conflicts to declare.

List of symbols and abbreviations

Symbols

ΔH^0	Standard enthalpy change, kJ mol^{-1}
η_{ch}	Chemical efficiency
η_{el}	Stoichiometric relation O_2/H_2 consumption, %
λ	Air-fuel equivalence ratio
ϕ	Relation between hydrogen supply from biogas/from electrolysis
$\dot{n}_i$	Molar flow rate of component i, mol s^{-1}
$X_{C,sp}$	Carbon conversion (specific), %
$X_{C,tot}$	Total carbon conversion, %
x_i	Mole fraction of component i

Abbreviations

ATR	Auto-thermal reforming
COR	Carbon conversion ratio, %
GHSV	Gas hourly space velocity, h^{-1}
MeOH	Methanol
r_{recy}	Recycle ratio
S/C	Steam-to-carbon ratio
SN	Stoichiometric number

Data availability

Acknowledgements

Notes and references

1 T. A. Saleh, *Bioresour. Technol. Rep.*, 2024, **25**, 101771.
2 M. Shahbaz, A. AlNouss, I. Ghiat, G. Mckay, H. Mackey, S. Elkhalifa and T. Al-Ansari, *Resour., Conserv. Recycl.*, 2021, **173**, 105734.
3 M. Dotzauer, T. Barchmann, U. Schmieder, N. Rensberg, W. Stinner, K. Arnold and C. Krüger, Kurzstudie zur Rolle von Biogas für ein klimaneutrales, 100% erneuerbares Stromsystem, 2035, **https://www.dbfz.de/fileadmin/ user_upload/Referenzen/Studien/ Kurzstudie_Biogas_2022.pdf**.
4 N. C. Joshi, S. Sinha, P. Bhatnagar, Y. Nath, B. Negi, V. Kumar and P. Gururani, *Curr. Res. Microb. Sci.*, 2024, **6**, 100237.
5 R. Suresh, L. Gnanasekaran, S. Rajendran, A. A. Jalil, M. Soto-Moscoso, K. S. Khoo, Z. Ma, H. S. Halimatul Munawaroh and P. L. Show, *Chemosphere*, 2023, **343**, 140173.
6 V. Pradeshwaran, V. Sundaramoorthy and A. Saravanakumar, *Biomass Bioenergy*, 2024, **188**, 107336.
7 D. Singh, P. Sirini and L. Lombardi, *Energies*, 2025, **18**, 15.
8 D. T. Troiano, T. Hofmann, S. Brethauer and M. H.-P. Studer, *Curr. Opin. Biotechnol.*, 2023, **81**, 102942.
9 C. Zhang, K.-W. Jun, R. Gao, G. Kwak and H.-G. Park, *Fuel*, 2017, **190**, 303–311.
10 S. Sollai, A. Porcu, V. Tola, F. Ferrara and A. Pettinau, *J. CO2 Util.*, 2023, **68**, 102345.

11 S. Bube, L. Sens, C. Drawer and M. Kaltschmitt, *Energy Convers. Manage.*, 2024, **304**, 118220.

12 S. Dabir, M. Cao, R. Prosser and T. Tsotsis, *Ind. Eng. Chem. Res.*, 2017, **56**, 1186–1200.

13 R.-Y. Chein, W.-H. Chen, H. Chyuan Ong, P. Loke Show and Y. Singh, *Chem. Eng. J.*, 2021, **426**, 130835.

14 F. Rau, A. Herrmann, H. Krause, D. Fino and D. Trimis, *Int. J. Hydrogen Energy*, 2019, **44**, 19135–19140.

15 R. Rinaldi and C. G. Visconti, *Chem. Eng. Sci.*, 2023, **272**, 118611.

16 R. Zuloeta Bonilla and R. Bhandari, *Energies*, 2022, **15**, 9329.

17 E. Moioli and T. Schildhauer, *Ind. Eng. Chem. Res.*, 2022, **61**, 7335–7348.

18 V. Kharitonov, V. Geza, L. Rodin and M. Shorohov, *Latv. J. Phys. Tech. Sci.*, 2023, **60**, 35–43.

19 P. Kenkel, T. Wassermann and E. Zondervan, *Processes*, 2021, **9**, 1348.

20 M. Pérez-Fortes, J. C. Schöneberger, A. Boulamanti and E. Tzimas, *Appl. Energy*, 2016, **161**, 718–732.

21 M. Rivarolo, D. Bellotti, L. Magistri and A. F. Massardo, *Int. J. Hydrogen Energy*, 2016, **41**, 2105–2116.

22 G. Iaquaniello, G. Centi, A. Salladini, E. Palo, S. Perathoner and L. Spadaccini, *Bioresour. Technol.*, 2017, **243**, 611–619.

23 B. Hernández and M. Martín, *Ind. Eng. Chem. Res.*, 2016, **55**, 6677–6685.

24 L. B. Braga, J. L. Silveira, M. E. da Silva, C. E. Tuna, E. B. Machin and D. T. Pedroso, *Renewable Sustainable Energy Rev.*, 2013, **28**, 166–173.

25 J. F. González, C. M. Álvez-Medina and S. Nogales-Delgado, *Energies*, 2023, **16**, 6343.

26 R. Kumar, A. Kumar and A. Pal, *Int. J. Hydrogen Energy*, 2022, **47**, 34831–34855.

27 L. Szablowski, M. Wojcik and O. Dybinski, *Energy*, 2025, **316**, 134540.

28 H. Park and P. Grundmann, *Energy Res. Social Sci.*, 2025, **119**, 103820.

29 W. Britz and R. Delzeit, *Energy Policy*, 2013, **62**, 1268–1275.

30 F. Rau, A. Herrmann, C. Dorn, H. Krause, S. Montenegro and D. Fino, *14. Symposium Energieinnovation*, 2016.

31 F. Nestler, M. Krüger, J. Full, M. J. Hadrich, R. J. White and A. Schaadt, *Chem. Ing. Tech.*, 2018, **90**, 1409–1418.

32 S. Rabe, T.-B. Truong and F. Vogel, *Appl. Catal., A*, 2007, **318**, 54–62.

33 M. Luneau, Y. Schuurman, F. C. Meunier, C. Mirodatos and N. Guilhaume, *Catal. Sci. Technol.*, 2015, **5**, 4390–4397.

34 V. Rathod and P. V. Bhale, *Energy Proc.*, 2014, **54**, 236–245.

35 F. Guerrero, L. Espinoza, N. Ripoll, P. Lisbona, I. Arauzo and M. Toledo, *Front. Chem.*, 2020, **8**, 145.

36 Z. Hou, J. Gao, J. Guo, D. Liang, H. Lou and X. Zheng, *J. Catal.*, 2007, **250**, 331–341.

37 A. Di Nardo, M. Portarapillo, D. Russo and A. Di Benedetto, *Int. J. Hydrogen Energy*, 2024, **55**, 1143–1160.

38 R. Pérez-Hernández, A. Gutiérrez-Martínez, J. Palacios, M. Vega-Hernández and V. Rodríguez-Lugo, *Int. J. Hydrogen Energy*, 2011, **36**, 6601–6608.

39 H. Nourbakhsh, J. Rahbar Shahrouzi, A. Zamaniyan, H. Ebrahimi and M. R. Jafari Nasr, *Int. J. Hydrogen Energy*, 2018, **43**, 15703–15719.

40 S. T. Wismann, J. S. Engbæk, S. B. Vendelbo, W. L. Eriksen, C. Frandsen, P. M. Mortensen and I. Chorkendorff, *Chem. Eng. J.*, 2021, **425**, 131509.

41 J. Schittkowski, B. Zeidler-Fandrich, T. Müller, R. Schlögl and H. Ruland, *Chem. Ing. Tech.*, 2022, **94**, 1397–1404.

42 P. Fosbol, Biogas to be converted into methanol, 2020, https://www.dtu.dk/english/news/all-news/nyhed?id=0efd777e-fa21-4d15-af01-c50d2512e14f.

43 J. Schipek, M. Kühn, H. Tauchnitz and F. Mertens, Methanolherstellung aus Biogas mittels Dreiphasenreaktor: (COOMet), https://gwf-gas.de/wp-content/uploads/2021/07/GE_07-08_2021_fb_Shipek.pdf.

44 A. R. Akhunyanov, P. A. Vlasov, V. N. Smirnov, A. V. Arutyunov and V. S. Arutyunov, *Kinet. Catal.*, 2024, **65**, 421–439.

45 K. Chouhan, S. Sinha, S. Kumar and S. Kumar, *Int. J. Hydrogen Energy*, 2021, **46**, 26809–26824.

46 European Parliament, *Directive 2014/68/EU of the European Parliament and of the Council on the Harmonisation of the Laws of the Member States Relating to the Making Available on the Market of Pressure Equipment: Pressure Equipment Directive*, 2014.

47 C. Fritsch, J. Dornseiffer, J. Blankenstein, M. Noyong, C. Groteklaes and U. Simon, *ChemCatChem*, 2024, **16**, 1–14.

48 T. Tsujiguchi, T. Furukawa and N. Nakagawa, *J. Power Sources*, 2011, **196**, 9339–9345.

49 P. Liu, J. Guo, H. G. Im and W. L. Roberts, *Combust. Flame*, 2023, **258**, 112379.

50 V. Dieterich, A. Buttler, A. Hanel, H. Spliethoff and S. Fendt, *Energy Environ. Sci.*, 2020, **13**, 3207–3252.

51 F. Nestler, J. Voß, A. Fastabend, T. Niemeier, H. Ruland and M. J. Hadrich, *Chem. Ing. Tech.*, 2024, **96**, 1166–1176.

52 M. Bukhtiyarova, T. Lunkenbein, K. Kähler and R. Schlögl, *Catal. Lett.*, 2017, **147**, 416–427.

53 D. S. Marlin, E. Sarron and Ó. Sigurbjörnsson, *Front. Chem.*, 2018, **6**, 446.

54 V. G. Rakhi and F. Mauss, *React. Kinet., Mech. Catal.*, 2023, **136**, 1197–1210.

55 S. Wang, Y. Wang, L. Yao and C. Hu, *Appl. Catal., B*, 2023, **333**, 122756.

56 Safe Start Up and Shut Practices for Steam Reformers: Doc 185/20, https://www.eiga.eu/uploads/documents/DOC185.pdf.

57 B. Hrycak, J. Mizeraczyk, D. Czylkowski, M. Dors, M. Budnarowska and M. Jasiński, *Sci. Rep.*, 2023, **13**, 2204.

58 L. Salano, M. M. Bozzini, S. Caspani, G. Bozzano and F. Manenti, *Processes*, 2024, **12**, 1598.

59 X. Zhao, B. Joseph, J. Kuhn and S. Ozcan, *iScience*, 2020, **23**, 101082.

60 J. Zhong, X. Yang, Z. Wu, B. Liang, Y. Huang and T. Zhang, *Chem. Soc. Rev.*, 2020, **49**, 1385–1413.

61 M. Hanifa, R. Agarwal, U. Sharma, P. C. Thapliyal and L. P. Singh, *J. CO_2 Util.*, 2023, **67**, 102292.

62 J. Skrzypek, M. Lachowska, M. Grzesik, J. Słoczyński and P. Nowak, *Chem. Eng. J. Biochem. Eng. J.*, 1995, **58**, 101–108.

63 J.-F. Portha, K. Parkhomenko, K. Kobl, A.-C. Roger, S. Arab, J.-M. Commenge and L. Falk, *Ind. Eng. Chem. Res.*, 2017, **56**, 13133–13145.

64 S.-A. Theofanidis, K. Stergiou, E. Delikonstantis and G. D. Stefanidis, *Ind. Eng. Chem. Res.*, 2024, **63**, 12035–12052.

65 O.-S. Joo, K.-D. Jung, I. Moon, A. Y. Rozovskii, G. I. Lin, S.-H. Han and S.-J. Uhm, *Ind. Eng. Chem. Res.*, 1999, **38**, 1808–1812.

66 S. Mucci, A. Mitsos and D. Bongartz, *J. Energy Storage*, 2023, **72**, 108614.

67 R. Rinaldi, G. Lombardelli, M. Gatti, C. G. Visconti and M. C. Romano, *J. Cleaner Prod.*, 2023, **393**, 136259.

68 J. S. Lee, S. H. Han, H. G. Kim, K. H. Lee and Y. G. Kim, *Korean J. Chem. Eng.*, 2000, **17**, 332–336.